Available online at www.eccomasproceedia.org
Eccomas Proceedia COMPDYN (2025) 481- 49

ECCOMAS
Proceedia

COMPDYN 2025
10th ECCOMAS Thematic Conference on
Computational Methods in Structural Dynamics and Earthquake Engineering
M. Papadrakakis, M. Fragiadakis (eds.)
Rhodes Island, Greece, 15-18 June 2025

A PARAMETRIC STUDY ON FRICTION PENDULUM SYSTEMS FOR BASE-ISOLATED BUILDINGS: INSIGHTS INTO PERFORMANCE ACROSS SEISMIC INTENSITIES

Livia Fabbretti[1], Eleni Chatzi[2], Filippo Ubertini[3], and Marco Breccolotti[3]

[1] Department of Civil and Environmental Engineering, University of Perugia
Via Goffredo Duranti, 93, 06125 Perugia, Italy
livia.fabbretti@dottorandi.unipg.it

[2] Department of Civil, Environmental, and Geomatic Engineering, ETH Zürich
Stefano-Franscini-Platz, 5, 8093 Zürich, Switzerland
chatzi@ibk.baug.ethz.ch

[3] Department of Civil and Environmental Engineering, University of Perugia
Via Goffredo Duranti, 93, 06125 Perugia, Italy
{filippo.ubertini, marco.breccolotti}@unipg.it

Abstract

Friction Pendulum Systems (FPS) are widely utilized in modern seismic protection. Although FPS have demonstrated their effectiveness in high-intensity seismic events, it is crucial to evaluate their performance in low-intensity earthquakes, where the system may not activate. This study proposes a parametric analysis of the seismic response of a base-isolated building, focusing on the influence of key parameters such as friction coefficient, initial stiffness, and rate parameter. The research is relevant because isolator manufacturers typically specify parameter ranges rather than exact values, while existing literature explores various empirical methods for estimating initial stiffness. Additionally, FPS can experience performance degradation over time due to aging and wear, highlighting the importance of continuous monitoring. The analysis is based on a real case study and employs a finite element model to simulate structural behavior under high and low-intensity seismic events. The analysis results with high-intensity earthquakes will allow for more accurate modeling of the isolators, providing refined parameter data. However, the study also highlights the challenges posed by events of low or moderate intensity, where the sliding of the isolators is not activated, requiring improved future strategies for system monitoring and data interpretation.

Keywords: Friction pendulum, Seismic intensity, Parametric investigation, Monitoring.

ISSN:2623-3347 © 2025 The Authors. Published by Eccomas Proceedia.
Peer-review under responsibility of the organizing committee of COMPDYN 2025.
doi: 10.7712/120125.12668.250 2

1 INTRODUCTION

1.1 Seismic isolation

Seismic isolation is one of the most widely adopted methods for passive control of the dynamic response of a building and serves as an effective solution for mitigating seismic damage. The decoupling of ground motion from structural movement significantly reduces the dynamic input to the structure. As a result, only a small portion of seismic energy is transferred to the superstructure. Part of the input energy is dissipated by the isolators through large displacements, that engage in their nonlinear behavior. This mechanism allows the structure to behave almost like a rigid body, experiencing reduced forces that can be sustained within the elastic field without damage.

Currently, two main types of isolators exist: elastomeric-based devices and friction-based devices. Elastomeric isolators are composed of vulcanized rubber layers interspersed with steel reinforcing plates. Friction-based isolators, on the other hand, consist of sliding surfaces, typically made of Teflon and steel, which can be either flat or curved. Among these, Friction Pendulum Systems (FPS) are the most adopted today and are available in single, double, or triple-pendulum configurations.

Research on base-isolated structures has demonstrated the excellent performance of isolation systems, particularly under high-intensity seismic events [1, 2]. However, other studies have highlighted the need to evaluate the behavior of isolated structures during low-energy ground motions. In such scenarios, the isolation system may not be activated, potentially preventing the intended decoupling effect [3, 4, 5, 6, 7]. Additionally, the behavior of seismic isolators is influenced by specific parameters, such as friction coefficient, initial stiffness, and rate parameter, that exhibit significant variability and cannot be predetermined. This variability introduces considerable uncertainty in predicting isolator performance.

To address these above-described challenges, this study investigates the variability in the seismic response of a real base-isolated building equipped with FPS. The analysis considers variations in key parameters of the isolation system across different seismic intensities. This parametric study provides valuable insights into the complex behavior of FPS-isolated structures under a wide range of scenarios.

A structural monitoring system will be installed in the case study building, offering a unique opportunity to validate theoretical models using real-world performance data.

1.2 Friction Pendulum System

The FPS operates based on the “pendulum principle” and its oscillation period depends solely on the equivalent radius of curvature. The stiffness of the isolator is primarily determined by the radius of the curved surfaces, while damping is provided by the dynamic friction coefficient between the sliding surfaces. Additionally, the curvature facilitates the recentering of the device after a seismic event. The advantage of using double or triple-pendulum devices is that a smaller isolator can achieve the same maximum displacement, as it utilizes the displacement of all curved surfaces.

In this study, the installed isolation system consists of ISOSISM® PS double-friction isolators, manufactured by Freyssinet. These are metallic devices designed with two curved sliding surfaces, between which a curved intermediate lens slides. A special sliding material called ISOGLIDE® (a Teflon-based polymer) is used between these elements to enhance the friction and energy dissipation properties of the device [8].

To model the behavior of this type of isolator in a finite element framework, it is necessary to define the following parameters, some of which are provided by producers and identified based on empirical observations:

- N_{sd} axial force acting on the isolator under quasi-permanent load combination.
- K_V vertical stiffness of the isolator, defined by manufacturers as:

$$K_V = N_{max}/(0.001 \div 0.003) \tag{1}$$

where N_{max} is the maximum axial force that the isolator can withstand and $0.001 \div 0.003$ represents the collapse shortening of the device in meters.

- μ_{fast} high-speed friction coefficient of the isolator, defined by manufacturers as:

$$\mu_{fast} = 0.04 \div 0.11 \tag{2}$$

- μ_{slow} low-speed friction coefficient of the isolator, defined by manufacturers as:

$$\mu_{slow} = (0.60 \div 0.70) \cdot \mu_{fast} \tag{3}$$

- R_{eq} equivalent radius of curvature. For single-curvature FPS isolators, this radius closely matches the geometric radius of curvature of the surface, while for double-curvature FPS isolators, it approximately equals twice the geometric radius of curvature for each curved surface.
- rp rate parameter. It quantifies how friction coefficients vary between static and dynamic states depending on sliding speed during motion. It is defined by manufacturers as:

$$rp = 0.02 \div 0.05 \tag{4}$$

- K_1 initial horizontal stiffness. It is used to model nonlinear behavior of the isolator, in both *x* and *y* directions, defined as:

$$K_1 = a_K \cdot K_2 \tag{5}$$

where K_2 is equal to N_{sd}/R_{eq}. Various values for a_K have been proposed in the literature based on experimental evaluations of FPS isolators. For instance, Naeim and Kelly [9] proposed a_K values of 51 and 150, depending on the geometric proportions of the devices. Dicleli [10] adopted an a_K value of 100, specifically in the context of seismic isolation for bridges. Cheng [11] assumed a_K to be 23.7, also in relation to bridge isolators characterized by large dimensions. Finally, Berto [12] suggested an a_K value of 600 for bridge isolation systems utilizing traditionally sized isolators.

- K_{eff} effective stiffness. It is used to model linear behavior of the isolator, in both *x* and *y* directions, defined as:

$$K_{eff} = N_{sd}/R_{eq} + \mu_{fast} \cdot N_{sd}/d_{max} \tag{6}$$

where d_{max} represents the maximum effective deformation of the isolator.

The study presented in this article stems from a critical analysis of Equations (1)-(6), which reveals that parameters governing FPS isolator behavior include coefficients that exhibit significant experimental variation over wide ranges. The substantial dispersion observed in these coefficients raises fundamental questions about how these empirical variables influence performance. Specifically, this research focuses on systematically quantifying how selecting specific coefficients within proposed ranges can alter isolator response and force distribution transmitted to the superstructure during seismic events of relatively high and low intensity. The methodological approach combines parametric sensitivity analysis with a nonlinear finite element model to establish quantitative relationships between variations in constitutive coefficients and structural performance indicators.

2 BASE-ISOLATED BUILDING UNDER INVESTIGATION

The building analyzed in this study is a reinforced concrete frame structure with seismic base isolation, housing the Guglielmo Marconi Scientific and Artistic High School in Foligno (Perugia, Italy). A detailed finite element model of the building was developed using SAP 2000 software [13] (Figure 1a).

The structure consists of four above-ground floors with deep pile foundations. To implement the seismic isolation system, a supporting substructure made of squat pillars was constructed, upon which thirty-eight isolators were installed. The isolation system is thus placed between the pilotis level and the first floor. The slabs are prefabricated predalles type.

Four types of ISOSISM® PS isolators were employed in the school complex, arranged according to the layout shown in Figure 1b. These isolator types differ in terms of maximum axial force capacity (N_{max}) and theoretical horizontal displacement (δ_{max}), while sharing the same equivalent radius of curvature, equal to 2.5 m. In the parametric investigation, N_{sd} for each isolator type was assumed to be equal to the average value of this parameter across all isolators of the same type (Table 1). This approach effectively reduced the analysis to four representative isolators rather than thirty-eight individual units, allowing the behavior of each isolator type to be considered independently of its specific location – an approximation deemed acceptable for this study. This methodology significantly improved computational efficiency without compromising the overall validity of the parametric evaluation.

3 PARAMETRIC INVESTIGATION

In this parametric analysis, the following parameters were systematically varied: high-speed friction coefficient (μ_{fast}), rate parameter (rp), and initial stiffness coefficient (a_K). Discrete values within predefined ranges were assigned to these parameters, resulting in a total of 100 combinations for the analysis:

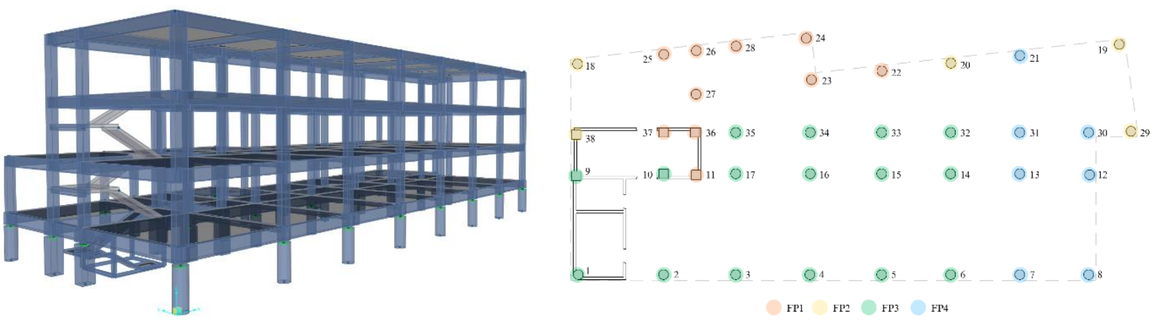

(a) (b)

Figure 1: The G. Marconi school building: (a) SAP 2000 model, (b) Layout of ISOSISM® PS isolators.

Bearing name	Bearing type	N_{max} [kN]	δ_{max} [m]	R_{eq} [m]	N_{sd} [kN]
FP1	ISOSISM® PS 1800.550	1800	± 0.275	2.5	701.40
FP2	ISOSISM® PS 1800.780	1800	± 0.390	2.5	807.28
FP3	ISOSISM® PS 3250.600	3250	± 0.300	2.5	1759.49
FP4	ISOSISM® PS 3250.740	3250	± 0.370	2.5	1572.91

Table 1: Key mechanical and geometric properties of the four ISOSISM® PS isolator types.

- a_K = 25; 50; 100; 200; 500
- μ_{fast} = 0.04; 0.06; 0.08; 0.10; 0.12
- rp = 0.02; 0.03; 0.04; 0.05

The low-speed friction coefficient (μ_{slow}) was not investigated due to its narrow range of variation defined in Equation (3). Instead, it was assumed to be equal to 65% of μ_{fast}.

Regarding the vertical stiffness (K_V), this parameter was kept constant, using 0.002 m in Equation (1), as the vertical component of seismic motion, although included in the modeling, is not significant for the study site. Consequently, vertical displacements are expected to be negligible.

A critical challenge arose with effective stiffness (K_{eff}), as the maximum deformation of the isolator (d_{max}) could not be predetermined. This necessitated the development of a formulation where K_{eff} depends on the values assumed for μ_{fast}.

3.1 CLS spectrum-compatible ground motion accelerograms

The formulation of K_{eff} and subsequent parametric analyses were initially performed by subjecting the structure to 7 spectrum-compatible ground motion accelerograms at Collapse Limit State (CLS), as indicated by the current design standard (NTC 2018 [14]). These artificial accelerograms (see, for example, Figure 2a) were generated using SIMQKE-1 software [15].

In this case, for K_{eff} formulation, an iterative computational procedure was implemented, starting with a preliminary assumed value of K_{eff} based on a plausible estimate of d_{max}. A Fast Nonlinear Analysis (FNA) was then performed [16], and the resulting d_{max} was calculated, refining the initial K_{eff} value. This process iteratively adjusted K_{eff} until convergence – defined as agreement between the assumed and calculated d_{max} – was achieved. In this analysis, rp = 0.03 was adopted as a central value within the range of variation of this parameter – which is an approximation but later found to have minimal impact on the behavior of the isolation system.

The methodology revealed an almost linear relationship between μ_{fast} and K_{eff} under spectrum-compatible seismic inputs, as illustrated in Figure 2b. As a result, a single slope derived from the trend line of this graphical relationship was adopted for subsequent analyses, simplifying parametric evaluation by leveraging the observed linear proportionality. This approach effectively decouples stiffness characterization from deformation uncertainties – a persistent limitation in conventional FPS isolator design methodologies.

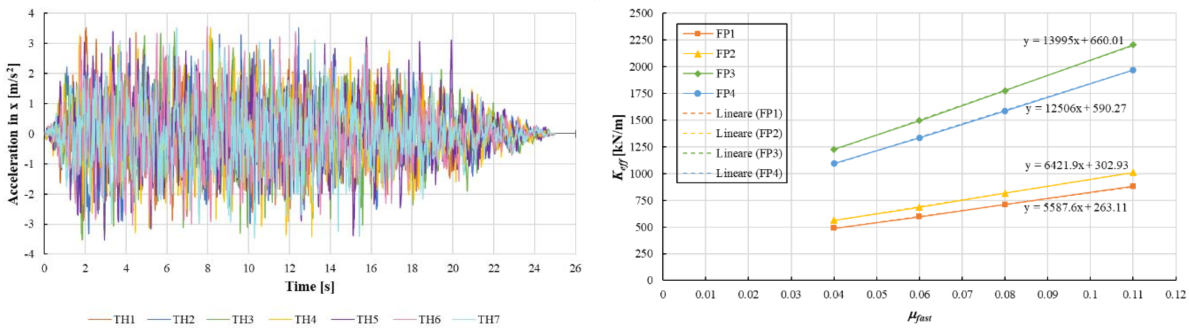

(a) (b)

Figure 2: (a) Spectrum-compatible ground motion accelerograms in the *x* direction, (b) Correlation between μ_{fast} and K_{eff} under spectrum-compatible seismic inputs.

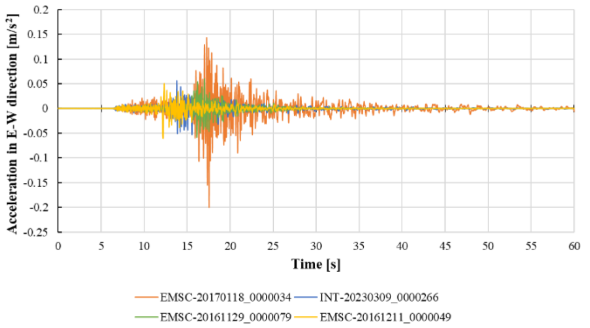

Figure 3: Accelerograms recorded in Foligno (East-West direction).

ID ITACA	Date	M_W	RE [km]	PGA [cm/s^2]
EMSC-20170118_0000034	2017-01-18	5.5	65.1	19.979
INT-20230309_0000266	2023-03-09	4.5	44.7	12.333
EMSC-20161129_0000079	2016-11-29	4.5	65.6	8.041
EMSC-20161211_0000049	2016-12-11	4.2	34.1	6.054

Table 2: Seismic events recorded in Foligno selected for performance evaluation.

3.2 Accelerograms of earthquakes occurred in Foligno

The formulation of K_{eff} and subsequent parametric analyses were then repeated by subjecting the structure to 4 accelerograms (Figure 3) recorded at the "Foligno Comando Carabinieri" station (code FOCC), the closest station to the building under study. These data, extracted from the ITACA (Italian Accelerometric Archive) database, include the most intense earthquake recorded in Foligno since 2009 and are associated with the 2016-2017 Central Italy seismic sequence and the 2023 Umbertide earthquake. The analysis was performed to evaluate the behavior of the base-isolated structure under real seismic events, which were significantly less intense compared to the requirements prescribed by the current design standard [14], with a peak ground acceleration of 19.98 cm/s² (see Table 2). The nonlinear nature of the structural response of the isolated building necessitated these additional analyses, as the relationship between input acceleration and structural response does not follow linear proportionality.

In this case, analytical results demonstrated that the seismic intensity associated with these events, and consequently the induced displacement field, was insufficient to activate sliding behavior in the isolation bearings, which maintained their structural response within the initial elastic phase. This observation led to the adoption of an effective stiffness, K_{eff}, equivalent to K_1 for each isolator in the computational model, as the devices did not exhibit a transition to nonlinear behavior under the examined ground motions.

4 RESULTS OF THE PARAMETRIC INVESTIGATION

4.1 CLS spectrum-compatible ground motion accelerograms

Figure 4 illustrates the results of the parametric analysis conducted using CLS spectrum-compatible accelerograms for the considered 100 combinations of the investigated parameters, in terms of isolator deformations and shear forces transmitted to the superstructure. The isolator deformations are calculated as the maximum absolute values of the vector sum of the relative displacements along the *x* and *y* axes, while the shear forces transmitted to the superstructure correspond to the maximum absolute values of the vector sum of their components along the same axes. The analysis highlights the influence of the parameters μ_{fast}, a_K, and rp on the dynamic response of FPS isolators.

An increase in the dynamic friction coefficient μ_{fast} (from 0.04 to 0.12) leads to a significant reduction in the relative displacements of the isolator (approximately 5 cm across all isolator types) and an increase in the transmitted force. This effect is attributed to greater energy dissipation due to friction. For isolators FP3 and FP4, which have higher capacity (N_{max} = 3250 kN), a non-monotonic behavior of shear force is observed, with an optimal minimum occurring at $\mu_{fast} \approx 0.06$.

The parameter a_K, which governs the initial stiffness K_1 through Equation (5), exhibits an inverse correlation with the maximum relative displacements of the isolator. Higher initial stiffness significantly reduces elastic deformation during the pre-sliding phase, thereby minimizing relative displacements between the superstructure and the base structure. However, regarding transmitted shear force, behavior varies depending on isolator type: FP1 and FP2 isolators display a nearly linear relationship, with shear forces decreasing as K_1 increases. Conversely, for FP3 and FP4 isolators, a critical threshold emerges at $\mu_{fast} \approx 0.08$. Beyond this threshold, the increase in effective stiffness (K_{eff}) due to frictional forces counterbalances stiffness reductions induced by K_1, resulting in increased resistance and reversing the trend observed below this value.

Finally, rp, which describes sliding velocity, is found to have a marginal impact on the dynamic response of FPS isolators. This finding suggests that combined effects of μ_{fast} and a_K are dominant in determining isolator behavior, allowing for simplification of numerical models by focusing optimization efforts on these key parameters.

Previous studies [17, 18] validate these results, emphasizing how optimal values of dynamic friction coefficients can significantly reduce structural stresses while enhancing energy dissipation.

Figure 5 presents the hysteresis loops for isolators 18 (type FP2) and 10 (type FP3). Isolator 18 exhibited the maximum displacement (0.297 m) in combination “1” (a_K = 25; μ_{fast} = 0.04; rp = 0.02), while isolator 10 transmitted the highest shear force (447.260 kN) in combination “100” (a_K = 500; μ_{fast} = 0.12; rp = 0.05). A comparative analysis of the graphs reveals hysteresis loops with distinctly different characteristics, attributable to the intrinsic properties of FP2 and FP3 isolators. Specifically, the hysteresis loop of the FP2 isolator is characterized by a linear trend with moderate slope, indicative of reduced stiffness, and a compact shape with limited internal area, suggesting minimal energy dissipation during cyclic motion. In contrast, the hysteresis loop of the FP3 isolator exhibits a steeper slope, denoting higher stiffness and greater energy dissipation capacity. This behavior aligns with the characteristic parameters of the two isolators: the lower horizontal stiffness of the FP2 isolator, correlated with lower N_{sd} and a_K values, implies a lower force required to induce lateral displacements, resulting in a more horizontal hysteresis loop. The reduced normal force in isolator 18 decreases the interlayer adhesion, facilitating lateral movements and contributing to a less inclined hysteresis loop. Furthermore, lower μ_{fast} values translate into hysteresis loops that extend more horizontally, with reduced vertical height. This highlights the fundamental trade-off in isolator design: displacement control is achieved at the expense of increased force transmission to the superstructure.

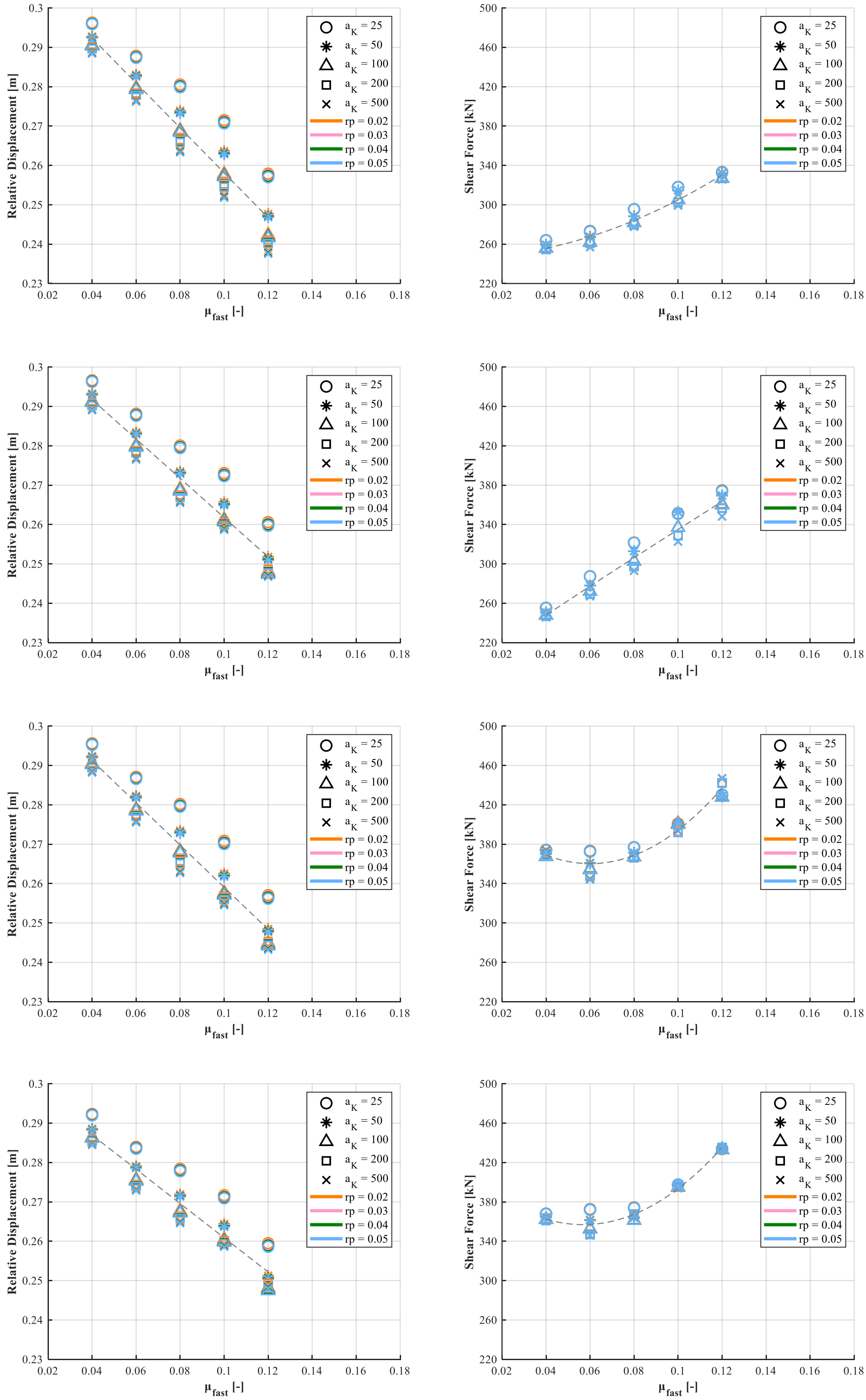

Figure 4: Relative displacements (left) and shear forces (right) as functions of μ_{fast}, a_K, and rp (first row FP1, second row FP2, third row FP3, fourth row FP4).

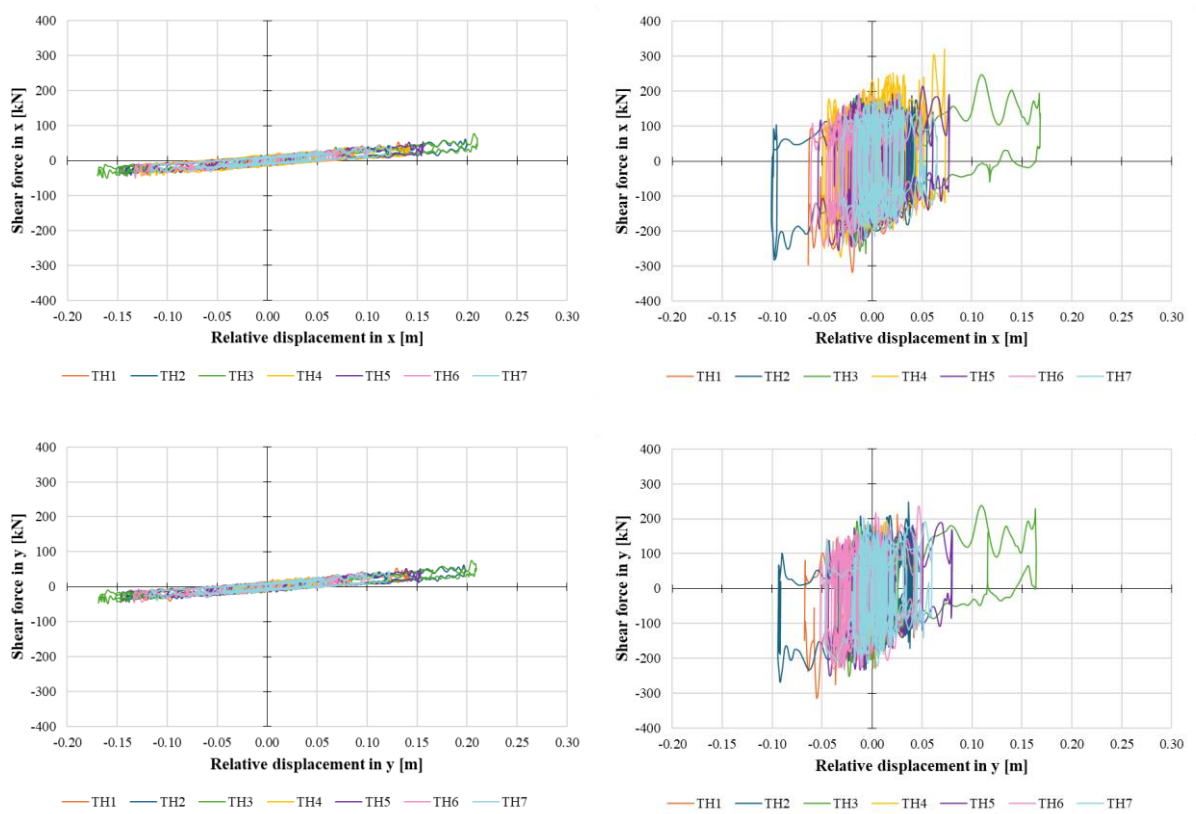

Figure 5: Hysteretic behavior of isolators in *x* (top) and *y* (bottom) directions: unit 18 (left), unit 10 (right).

4.2 Accelerograms of earthquakes occurred in Foligno

Figure 6 presents the results of the parametric analysis conducted using the accelerograms recorded in Foligno. Similarly to the previous analysis, isolator deformations and shear forces transmitted to the superstructure were considered for the 100 parameter combinations. In this context, the parameter rp has a marginal impact on the dynamic response of FPS isolators, as does μ_{fast}. This is evident from the fact that all graphs exhibit a substantially horizontal trend. The predominant parameter in determining the behavior of the isolators is instead a_K, which shows an inverse correlation between its value and the maximum relative displacements for all isolator types. Conversely, as a_K increases, so do the shear forces, except for the FP4 isolator. However, in the case of recorded earthquakes, the analyzed parameters do not significantly affect the behavior of the isolators, which deform but without ever activating sliding.

Figure 7 presents the hysteresis loops for isolators 29 (type FP2) and 9 (type FP3). Isolator 29 exhibited the maximum deformation (0.001 m) in combination “1” (a_K = 25; μ_{fast} = 0.04; rp = 0.02), while isolator 9 transmitted the highest shear force (46.666 kN) in combination “25” (a_K = 500; μ_{fast} = 0.12; rp = 0.02). The analysis of these graphs confirms the previous results, showing that none of the accelerograms is strong enough to activate the sliding in the FPS isolators, not even the “EMSC-20170118_0000034” earthquake, which is the strongest recorded in Foligno, even under combinations that maximize shear forces or deformations.

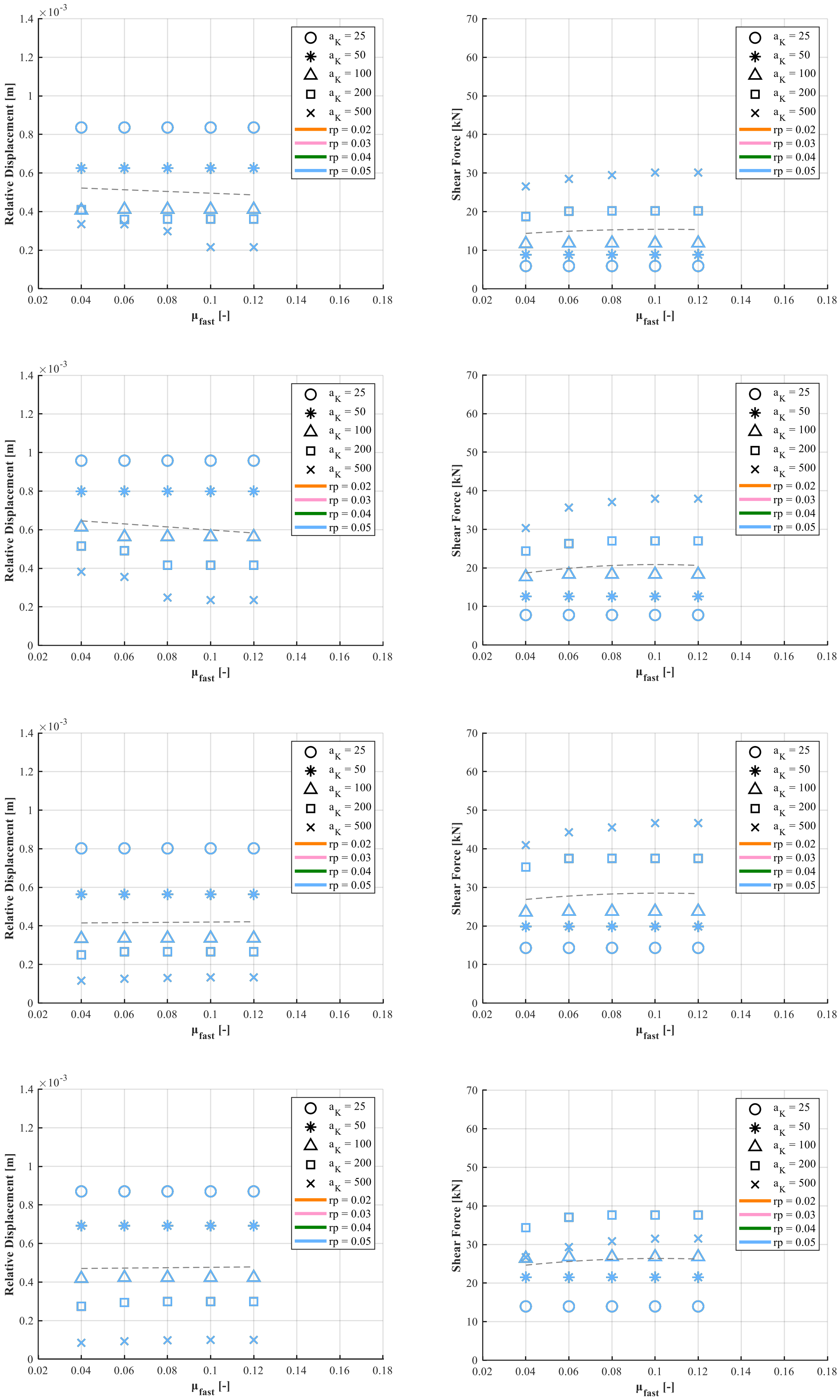

Figure 6: Relative displacements (left) and shear forces (right) as functions of μ_{fast}, a_K, and rp (first row FP1, second row FP2, third row FP3, fourth row FP4).

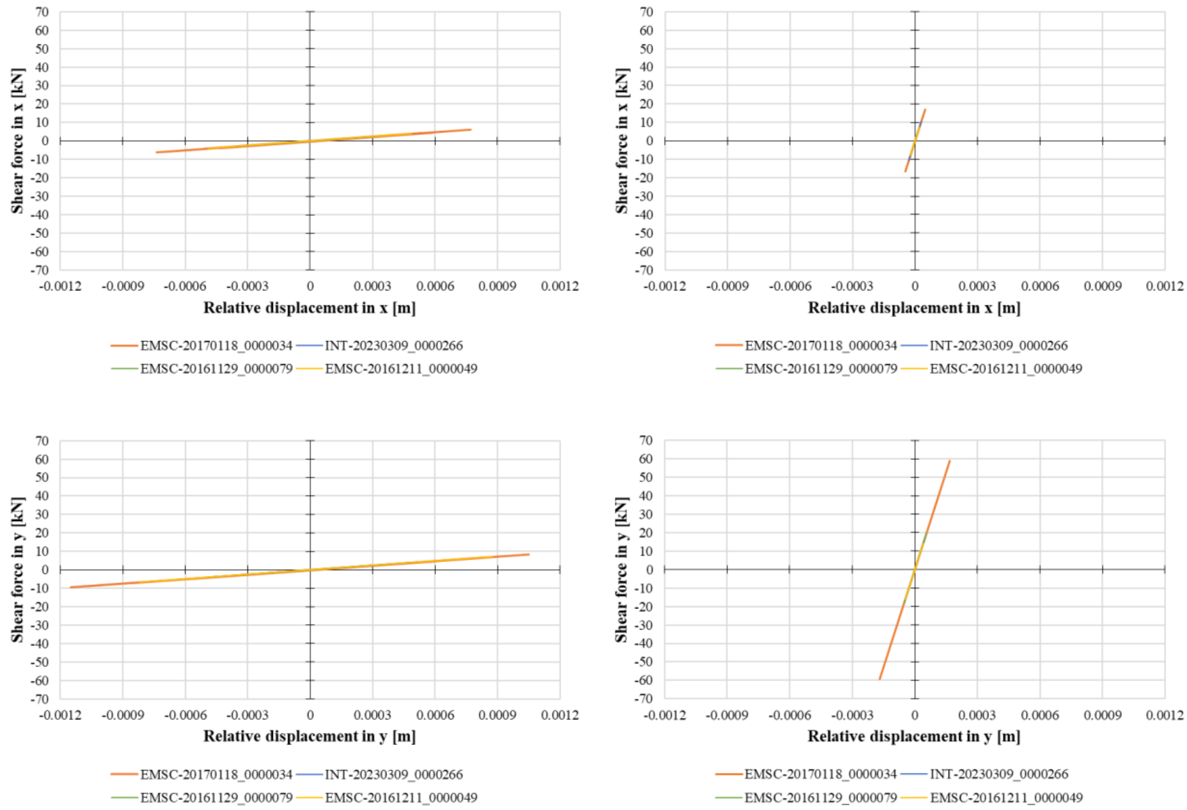

Figure 7: Hysteretic behavior of isolators in the *x* (top) and *y* (bottom) directions: unit 29 (left), unit 9 (right).

5 CONCLUSIONS

This work presents a parametric investigation aimed at evaluating the effects of uncertain design parameters on the behavior of FPS isolation systems subjected to seismic events of varying intensities. The study further identifies the operating conditions under which a seismic monitoring system can effectively detect and assess variations caused by damage, deterioration, or aging of the FPS seismic isolation system.

The results of the investigation confirm the significant influence of design parameters on the evaluation of maximum deformation of the isolation devices and maximum stresses in the structural elements. The findings underscore the challenges associated with monitoring the performance of FPS seismic isolation systems, suggesting that, in the absence of relatively high-intensity earthquakes, verifying the system's efficacy or detecting variations and damages may prove difficult. A monitoring system can provide valuable insights during a seismic sequence, which can be leveraged to predict the system's effectiveness in the event of a stronger aftershock.

Further research will in any case be necessary to explore whether other types of loads, such as wind action, could influence the activation of isolator sliding, offering new perspectives for validation, management, and monitoring of these systems.

ACKNOWLEDGEMENTS

The first author gratefully acknowledges the support of the Province of Perugia and the European Union through the NextGenerationEU program – National Recovery and Resilience Plan (PNRR) – for co-sponsoring his doctoral fellowship.

REFERENCES

[1] T. Saito, Behavior of response controlled and seismically isolated buildings during severe earthquakes in Japan. *Energia, Ambiente e Innovazione*, **5**, 31-37, 2015.

[2] M. Celebi, Successful performance of a base-isolated hospital building during the 17 January 1994 Northridge earthquake. *The Structural Design of Tall and Special Buildings*, **5**, 95-109, 1996.

[3] P. Clemente, G. Bongiovanni, G. Buffarini, F. Saitta, Experimental analysis of base-isolated buildings under low magnitude vibrations. *International Journal of Earthquake and Impact Engineering*, **1**, 199-223, 2016.

[4] A. Salvatori, A. Di Cicco, P. Clemente, Seismic monitoring of building with base isolation. *7th Int. Conference on Computational Methods in Structural Dynamics and Earthquake Engineering* (COMPDYN 2019), Crete, Greece, June 24-26, 2019.

[5] P. Clemente, A. Martelli, Seismically isolated buildings in Italy: State-of-the-art review and applications. *Soil Dynamics and Earthquake Engineering*, **119**, 471-487, 2019.

[6] P. Clemente, G. Bongiovanni, G. Buffarini, F. Saitta, M. G. Castellano, F. Scafati, Effectiveness of HDRB isolation systems under low energy earthquakes. *Soil Dynamics and Earthquake Engineering*, **118**, 207-220, 2019.

[7] F. Scafati, C. Ormando, P. Clemente, G. Buffarini, G. Bongiovanni, Effects of low energy earthquakes on a R.C. building seismically isolated by means of HDRBS and SDS. *18th World Conference on Earthquake Engineering*, Milan, Italy, June 30-July 5, 2024.

[8] Freyssinet, Technical product sheet ISOSISM® PS PENDULUM SYSTEMS. *Data sheet No.: FT En CV55 V01-06/24*.

[9] F. Naeim, J. M. Kelly, *Design of Seismic Isolated Structures: From Theory to Practice*, 1st Edition. John Wiley & Sons, 1999.

[10] M. Dicleli, S. Buddaram, Effect of isolator and ground motion characteristics on the performance of seismic-isolated bridges. *Earthquake Engineering and Structural Dynamics*, **35**, 233-250, 2006.

[11] F. Y. Cheng, H. Jiang, K. Lou, *Smart Structures: Innovative systems for seismic response control*, 1st Edition. CRC Press, 2008.

[12] L. Berto, T. Favaretto, A. Saetta, Seismic risk mitigation technique for art objects: Experimental evaluation and numerical modelling of double concave curved surface sliders. *Bulletin of Earthquake Engineering*, **11**, 1817-1840, 2013.

[13] Computers and Structures, Inc. (CSI), SAP2000 User's Manual (Version 22.0.0). *Computers and Structures, Inc. (CSI)*, 2020.

[14] Ministero delle Infrastrutture e dei Trasporti, Aggiornamento delle Norme Tecniche per le Costruzioni (NTC 2018). *Official Gazette of the Italian Republic*, **42**, 2018.

[15] E. H. Vanmarcke, C. A. Cornell, D. A. Gasparini, S. Hou, SIMQKE-1 User's Manual (Version 2.7). *The Earthquake Engineering Online Archive – NISEE e-Library*, 1976.

[16] Computers and Structures, Inc. (CSI), Fast Nonlinear Analysis (FNA). *Technical Knowledge Base*, 2016.

[17] D. Cancellara, F. De Angelis, Assessment and dynamic nonlinear analysis of different base isolation systems for a multi-storey RC building irregular in plan. *Computers and Structures*, **180**, 74-88, 2017.

[18] A. S. Vibhute, S. D. Bharati, M. K. Shrimali, T. K. Datta, Optimum Coefficient of Friction in FPS for Base Isolation of Building Frames. *Practice Periodical on Structural Design and Construction*, **27**, 1-14, 2022.